Desalination and Water Treatment
www.deswater.com

doi: 10.5004/dwt.2021.26718

213 (2021) 358–370
February

Adsorption of Cu(II) and Cr(III) ions on SBA-15 mesoporous silica functionalized by branched amine

Ying Yang[a], Xiang Cao[a], Zhenping Ma[a], Guohao Wu[a], Liangliang Zheng[a], Yuanyuan Zhang[a,b,*]

[a]*School of Chemical Engineering, Jiangsu Ocean University, Lianyungang 222005, China, email: zhangyy@jou.edu.cn*
[b]*Jiangsu Key Laboratory of Marine Bioresources and Environment, Jiangsu Ocean University, Lianyungang 222005, China*

Received 21 May 2020; Accepted 17 October 2020

ABSTRACT

SBA-15 mesoporous silica-bearing branched amine was explored as the adsorbent for the efficient removal of Cu(II) and Cr(III) ions from aqueous solutions. The nanoabsorbent was prepared by the Michael addition of amino-modified SBA-15 with methyl acrylate and subsequent amidation with diethylenetriamine (DETA). Batch tests were performed and the optimal adsorption pH was determined to be 5.0 for Cu(II) and 3.0 for Cr(III). The experimental data showed the adsorption process was well represented by both pseudo-second-order kinetic model and Langmuir isotherm model. According to the Langmuir equation, maximum Cu(II) and Cr(III) adsorption capacities of SBA-15-DETA were 57.5 and 48.3 mg g^{-1}, respectively, which were much higher than the values of amino-functionalized silica precursor. Furthermore, the adsorbent showed excellent stability and could be readily regenerated by acid treatment without an obvious reduction in adsorption efficiency. Thus, SBA-15-DETA prepared here shows great application prospects for the adsorption and recovery of aqueous heavy metal ions.

Keywords SBA-15 mesoporous silica; Branched amine; Adsorption; Cu(II); Cr(III)

1. Introduction

Heavy metal ions in environment are known to cause severe threat on the ecological systems and public health [1,2]. Among them, copper and chromium are often present in effluents of electroplating, leather tanning, and dyeing. These ions at a high level are toxic to living organisms and could enter and accumulate in human body tissues through food or drinking water, leading to a great variety of diseases and disorders. Many techniques including adsorption, membrane process, ion exchange, and precipitation have been explored to decontaminate water solutions from heavy metal ions [3]. Among them, adsorption is one of the most effective and widely used methods due to its high efficiency and simplicity for treatment. Most importantly, the adsorption process is generally reversible and adsorbent could be easily regenerated for use again, leading to the reduction of treatment cost [4,5].

With the advancement of materials chemistry, the mesoporous silica substrates have shown great potential for the metal ions removal application over the past decade, and this is due to the fact that mesoporous silica offers excellent adsorbent features such as good stability, uniform pore size, and relatively high surface area [6,7]. Furthermore, by reason of the high density of silanol on the internal pore surface of mesoporous silica, various functional groups could be easily immobilized after silane treatment [8–12]. Among the different mesoporous materials, SBA-15 has been

* Corresponding author.

regarded to be most promising for ions adsorption due to the advantages of higher thermal stability, higher mechanical strength, and larger pore size up to 30 nm in diameter as compared with other mesoporous silica sources [13].

It is worth mentioning that the nitrogen-containing ligands have a strong sorption affinity toward a variety of cations or anions at specific pH values [14]. Therefore, a considerable number of organic functional groups including amino [15], polyamine [16,17], imidazole [18], pyrazole [19], have been incorporated into mesoporous silica for chelation. The amine groups were generally added by the process of co-condensation or post-modification of the mesoporous silica matrix. For instance, the amino-functionalized SBA-15 materials with fibrous-like, rod-like, and platelet-like morphologies were obtained through co-condensation and their adsorption behaviors were studied and compared [20]. The mono-, di-, and tri-amine grafted SBA-15 materials have also been prepared by two independent methods and the adsorption results showed the adsorption capacity for Hg(II) increased with an increasing amount of nitrogen of coupling agents [16,17]. Besides, the amine molecule has been reported to graft on mesoporous materials by reacting with epoxy unit modified substrate [21]. For easily separation by an external magnet field, the amino-functionalized magnetic nanocomposites Fe_3O_4@SBA-15 were prepared and the adsorption of Pb(II) was studied [22]. Apart from the ions adsorption, amine-modified SBA-15 has also been explored as an adsorbent to remove organic pollutants such as pentachlorophenol [23].

It has been reported that the adsorption performance of porous materials is affected by the surface density of the grafted chelating groups [24,25]. In particular, dendrimeric ligands such as four carboxyl groups containing porphyrin [26], ethylenediaminetetraacetic acid (EDTA) [27], have been immobilized onto the mesoporous materials to improve adsorption capacity toward heavy metals. Poly(ethyleneimine) (PEI), which contains plenty of amine groups on the single macromolecular chain, has also been functionalized on the surface of porous silica for adsorption application [28,29]. In addition, multi-reactive groups containing compounds including cyanuric chloride [30,31] and benzenetricarbonyl trichloride [32] have been anchored on the mesoporous silica surface and served as the branched linker, to provide more reacting sites for the introduction of chelating groups. All results reveal the branched structure of ligands on the surface of mesoporous materials could increase sorption efficiency toward heavy metal ions.

The objective of this study was to develop the mesoporous silica adsorbent with the branched structure of ligands via facial post-synthesis functionalization for the adsorption and removal of metal ions. Based on the above considerations, branched amine-immobilized mesoporous silica SBA-15-DETA has been prepared via Michael addition of amino-modified SBA-15 with methyl acrylate (MA) and subsequent amidation with diethylenetriamine (DETA). Batch experiments were carried out and SBA-15-DETA was used as the solid-phase extraction adsorbent for removing Cu(II) and Cr(III) ions. Moreover, pH-dependent effect, adsorption kinetic models, adsorption isotherms, ionic strength, co-existing ions, and regeneration of SBA-15-DETA were also evaluated.

2. Materials and methods

2.1. Material

Toluene (Sinopharm Chemical Reagent, analytically pure) was dried with calcium hydride under reflux for 24 h and collected by distillation under reduced pressure. Pluronic P123 triblock copolymer was obtained from Sigma-Aldrich. Methyl acrylate (MA), 3-aminopropyltrimethoxysilane (APTMS), DETA, tetraethylorthosilicate (TEOS), methanol, ethanol, $CuSO_4{\cdot}5H_2O$, $Cr(NO_3)_3{\cdot}9H_2O$, NaCl, and $NaNO_3$ were all analytically pure and purchased from Sinopharm Chemical Reagent without further purification.

2.2. Characterization

Transmission electron microscopy (TEM) images were collected on JEOL JEM-1400 with 100 kV acceleration voltage. Scanning electron microscopy (SEM) image was obtained on SM-6390 (JEOL). The nitrogen adsorption–desorption isotherms were determined by specific surface area measuring instrument Beijing Beishide 3H-2000PM1. The Brunauer–Emmett–Teller (BET) model was employed for the analysis of specific surface areas. Although Barret–Joyner–Halenda (BJH) method is not the most accurate on the pore size distribution for mesoporous materials as compared with other proposed methods [33], it is still widely used due to the simplification. Finally, BJH method was adopted to evaluate pore size distribution in this study. Fourier transform infrared (FTIR) spectra were recorded on a Shimadzu Prestige-21 spectrometer. Quantitative determination of the concentrations of Cu(II) and Cr(III) was carried out by flame atomic absorption spectrometry (FAAS) Beijing Purkinje General TAS-990 with an air-acetylene flame. The thermal stability was studied using thermogravimetric analysis (TGA) analyzer GA Q500 in airflow at a heating rate of 10°C min^{-1}. To quantify the nitrogen content, elemental analysis (LECO TC400) was used.

2.3. Preparation of SBA-15-DETA

SBA-15 type mesoporous silica with Pluronic P123 copolymer as the surfactant template was synthesized according to the literature reported [34]. For the removal of the template, the prepared silica material was calcinated at 550°C for 6 h. After that, the template removed SBA-15 (4.0 g) was placed in a flask containing in anhydrous toluene (100 mL) and dispersed by sonication. Subsequently, APTMS (4.0 mL) was added and the suspension was heated at reflux for 24 h under a nitrogen atmosphere. After centrifugation, the resultant solid was isolated and washed three times with ethanol. Finally, the product was dried under vacuum and denoted as SBA-15-NH_2.

For coupling with MA, SBA-15-NH_2 (4.0 g) was added into the mixture of methanol (80 mL) and MA (6.0 mL) and dispersed by sonication. Then, the suspension was stirred to react at 50°C for 48 h under a nitrogen atmosphere. After centrifugation, the resultant solid SBA-15-MA was isolated, washed three times with ethanol, and dried under vacuum.

Finally, SBA-15-MA (3.8 g) was added into the methanol (80 mL) and dispersed by sonication. After the addition of

DETA (19 mL), the suspension was stirred to react at 50°C for 48 h under a nitrogen atmosphere. The resultant solid was isolated by centrifugation, washed three times with ethanol. After drying under vacuum, the resultant product was obtained and denoted as SBA-15-DETA.

2.4. Zeta potential measurement

For the measurement of zeta potential values, 0.01 g of SBA-15-DETA was dispersed in 100 mL of 0.1 mmol/L NaCl solution assisted by sonicator and the pH of suspension was adjusted by using HCl or NaOH solution was used for zeta potential measurement.

2.5. Adsorption experiments

Batch tests were performed to study the adsorption features of branched amine-immobilized SBA-15-DETA for the removal and concentration of Cu(II) and Cr(III) from water. The salt $CuSO_4 \cdot 5H_2O$ and $Cr(NO_3)_3 \cdot 9H_2O$ were dissolved in high purity water to prepare their corresponding metal ion stock solutions at the required concentration for experiments. The adsorbed amount Q (mg g^{-1}) was determined using the following expressing: $Q = (C_0 - C) \times V/W$, where C_0 and C define the initial and final concentration of targeted ions (mg L^{-1}), respectively, V refers to the volume (L) of the suspension, and W is the mass (g) of the SBA-15-DETA.

2.5.1. Effect of pH

40.0 mg of SBA-15-DETA was added to the 50 mL conical flask containing 40.0 mL of 100 mg L^{-1} of Cu(II) or Cr(III) solution. After that, the pH values of each suspension were adjusted with diluted HNO_3 or NaOH solutions to 2.0, 3.0, 4.0, 5.0, 6.0, 7.0, and 8.0. All the flasks were placed into the automatic shaker with a water bath and shaken at 25°C for 300 min to reach the equilibrium. After adsorption, the solid adsorbents were removed by filtration with a syringe filter (0.22 μm), and the concentration of heavy metal elements was determined by FAAS.

2.5.2. Effect of contact time

40.0 mg of SBA-15-DETA was added in the 40.0 mL of 100 mg L^{-1} Cu(II) or Cr(III) solution at the optimum pH values. Then, the suspensions were shaken in the automatic shaker at 25°C in the dark. At predetermined time intervals (1, 2, 4, 8, 16, 30, 60, 120, and 180 min), 2.0 mL of the suspension was taken out, the solid adsorbents were removed by filtration with syringe filter (0.22 μm), and the concentration of heavy metal elements was determined by FAAS.

2.5.3. Effect of initial concentration

Concentrations of ions solutions were prepared to be 20, 40, 60, 100, 140, 200, 300, and 400 mg L^{-1} at first. After adjusting the pH of solutions to the desired values, the 40.0 mL of the above ion solution and 40.0 mg of the absorbent were transferred into the conical flask and the flask was shaken at 25°C for 300 min. After the filtration with 0.22 μm syringe filter, the ion concentration of the filtrate was determined by FAAS.

2.5.4. Adsorption selectivity

The mixed ions solution containing seven metal cations including Cu(II), Cr(III), Co(II), Ni(II), Cd(II), Mn(II), and Na(I) was prepared at first and each ions solution was set as 100 mg L^{-1}. Experimental conditions were consistent with those in the effect of the initial concentration study.

2.5.5. Reusability study

Initially, the metal ion adsorbed SBA-15-DETA was isolated by centrifugation and the adsorbent was regenerated by treating with 0.1 mol L^{-1} HCl for 1 h two times. Subsequently, the ions-removed adsorbent was neutralized with 5% $NaHCO_3$ solution once for 0.5 h and washed with deionized water. Finally, four cycles of adsorption–desorption were conducted.

3. Results and discussion

3.1. Synthesis and characterization

The branched amine-modified mesoporous silica, SBA-15-DETA, was prepared via three steps (Fig. 1). At first, amino groups were immobilized onto the channel surface of template-removed SBA-15 by silylation, and then the addition of MA to the amino groups was realized via Michael reaction, resulting in the branched structure. Finally, DETA was reacted with ester groups by amidation to obtain the product SBA-15-DETA with the branched amine. SEM and TEM images of the product are shown in Fig. 2. The SEM image shows that SBA-15-DETA possessed short rod-like morphology with an average size of 0.5 μm in diameter. TEM images of SBA-15-DETA exhibit that mesoporous channels were homogeneously arranged. The results suggest that SBA-15-DETA maintained the well-ordered hexagonal mesoporous structure even after the multi-step chemical modifications.

The chemical modification of each synthetic step was monitored by FTIR spectra. It can be observed that the intense absorption peaks at 815 and 1,090 cm^{-1} were present in all samples (Fig. 3), and these peaks were attributed to the stretching vibration of Si–O–Si bond in the condensed silica network. In comparison to pristine SBA-15, a new peak from SBA-15-NH_2 appeared around 1,535 cm^{-1}, which could be due to the N–H bending vibration of the primary amine. Also, the appearance of a peak at 2,930 cm^{-1} was evidence of asymmetric C–H stretching in the propyl chain of APTMS, confirming silane coupling agent has been immobilized on the material. When SBA-15-NH_2 was treated with MA, a new and distinct peak at 1,743 cm^{-1} was observed, and it was in agreement with the C=O stretching vibration from the introduced ester bonds. After amidation with DETA, the peak at 1,743 cm^{-1} shifted to 1,725 cm^{-1} as to that of SBA-15-MA, indicating that the ester bond has turned into an amido group. Furthermore, the new peak appeared at 1,625 cm^{-1} was due to the stretching vibration mode of amine groups (primary and secondary), and the results indicate that the branched amine was successfully introduced.

The nitrogen adsorption–desorption isotherms were used to investigate the mesopore structure parameters and the curves are shown in Fig. 4. The isotherms of all samples

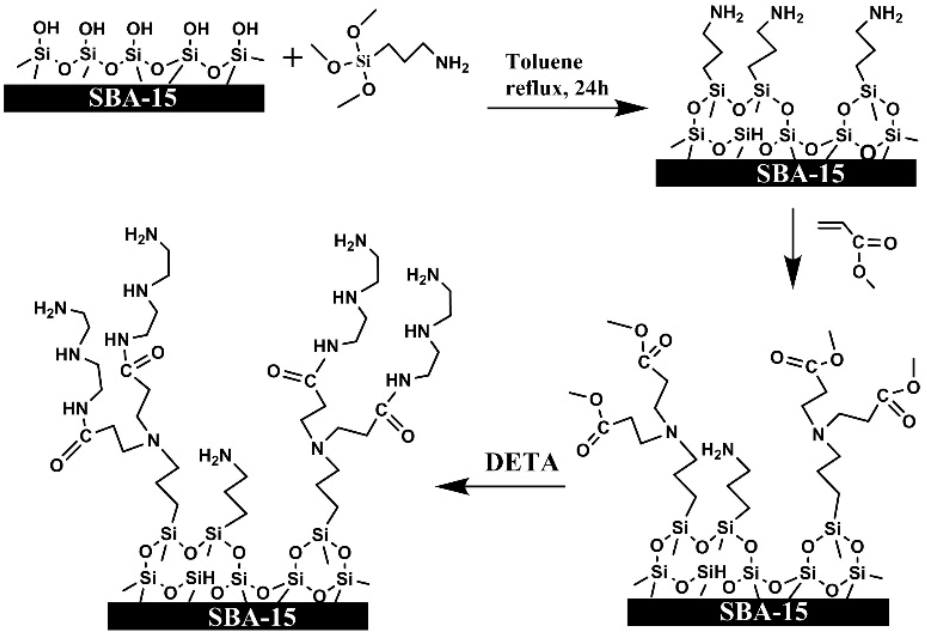

Fig. 1. Synthetic route of SBA-15-DETA.

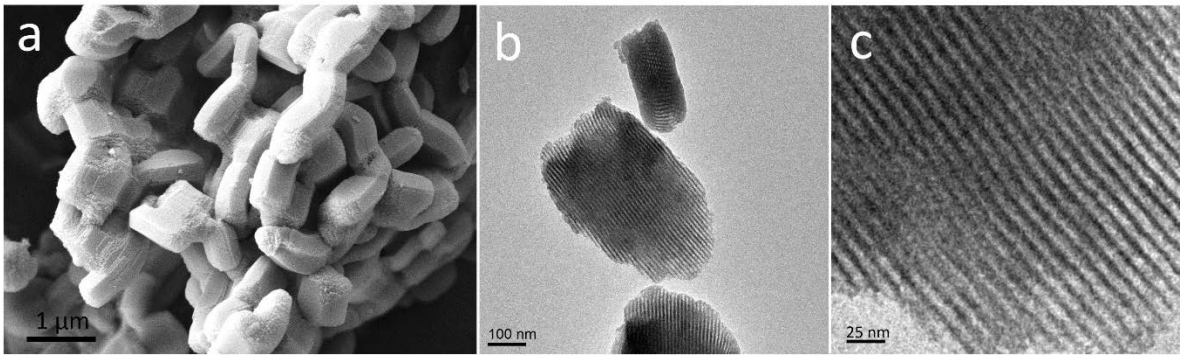

Fig. 2. SEM image (a), TEM image (b), and enlarged TEM image (c) of SBA-15-DETA.

exhibited characteristic type IV curves with H1 hysteresis loop in the partial pressure range of 0.5–0.8, indicating the presence of ordered cylindrical channel-like mesopores inside. The BET specific surface area and pore volume of SBA-15 were determined to be 485.1 and 0.528 mL g^{-1}, respectively, with a pore size distribution centered at 5.68 nm (Table 1). Besides, the BET surface area and pore volumes as well as average pore diameters decreased as modification proceeded step by step, due to the successful grafting of an organic constituent with the contraction of the mesopore channels. The pore size of SBA-15-DETA was still 4.35 nm, indicating the pore channels were still preserved after the modification process. There is no doubt that the relatively large pore size of SBA-15-DETA allowed easier diffusion of metal ions in and out of channels for adsorption.

The low-angle XRD data of SBA-15 and SBA-15-DETA are displayed in Fig. 5. The pristine SBA-15 exhibited a single strong peak indexed to the characteristic (100) diffraction line, followed by two additional weak peaks which were indexed to (110, 200) diffraction associated with hexagonal symmetry of the pores. After anchoring with the branched amine, the relative intensities of characteristic diffraction peaks decreased slightly because of the filling of some of the pores by the grafted ligands and the slight decrease of long-range order.

Typically, the silica materials are highly thermally stable, while the grafted organic component decomposes at high temperature to induce the weight loss of the composites after heating. Thus, TGA was used to evaluate the thermal stabilities and organic contents of all silica samples. As shown in Fig. 6, curves of TGA for all samples exhibited continuous and slow weight loss in the heating process. When the samples were heated at 800°C, the weight loss of the SBA-15 precursor was 1.9%. Since the pristine SBA-15 has been calcinated at 550°C, the slight weight loss was possibly attributed to the loss of some silanol groups at high temperatures. However, SBA-15-NH_2, SBA-15-MA, and SBA-15-DETA presented much higher weight losses of 12.6%, 19.9%, and 25.8%, respectively. The implication of the increasing weight losses of these samples is that the

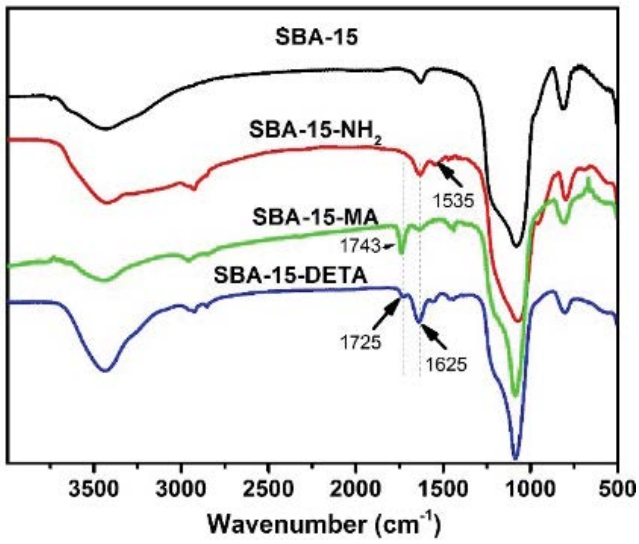

Fig. 3. FTIR spectra of the SBA-15 material and its derivatives.

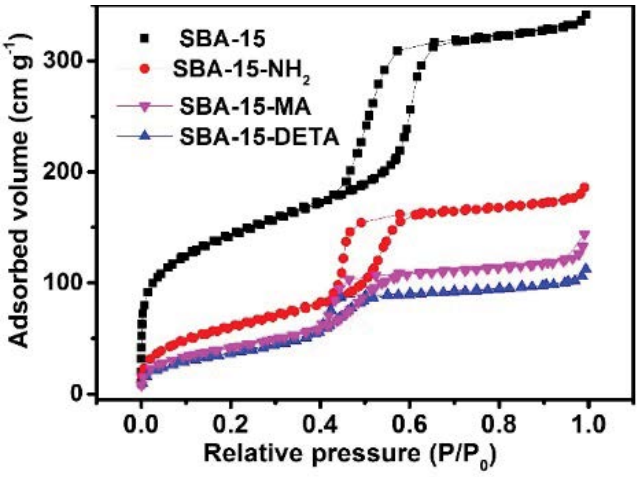

Fig. 4. Nitrogen adsorption–desorption isotherms of SBA-15 material and its derivatives.

Table 1
Structure parameters of SBA-15 material and its derivatives measured by nitrogen adsorption–desorption isotherm

Samples	BET surface area ($m^2\ g^{-1}$)	Pore volume ($mL\ g^{-1}$)	Pore size (nm)
SBA-15	485	0.528	5.68
SBA-15-NH_2	222	0.287	5.17
SBA-15-MA	156	0.222	4.99
SBA-15-DETA	139	0.174	4.35

organic contents of the adsorbents increased as modification proceeded stepwise. Moreover, the weight loss difference between SBA-15-MA and SBA-15-DETA was 5.9%, confirming the successful introduction of branched amine ligand.

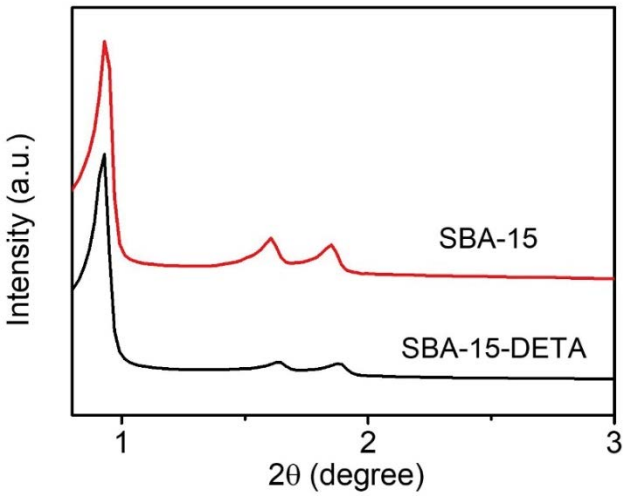

Fig. 5. Low-angle XRD patterns of SBA-15 and SBA-15-DETA.

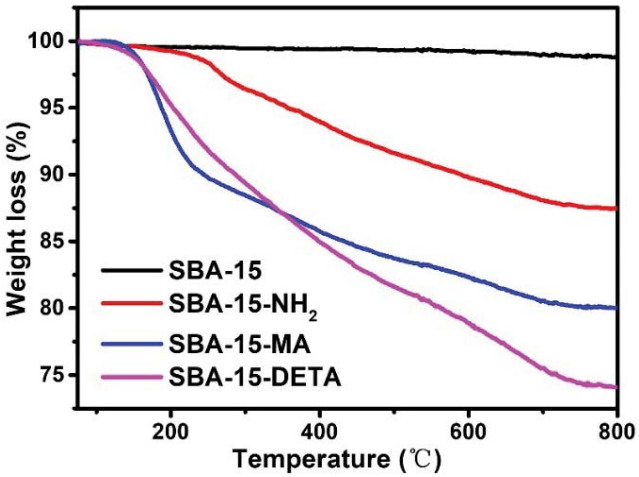

Fig. 6. TGA curves of SBA-15 and its derivatives.

3.2. Effect of pH

The solution pH is one major variable that determines the adsorption behavior and capability [35]. The apparent zeta-potential value of SBA-15-DETA at different pH values was studied. Fig. 7a reveals the potential value of SBA-15-DETA decreased accordingly with the increase in pH value of suspension. Meanwhile, the isoelectric point was determined at about the pH of 7.4 when the zeta potential was zero. Below this pH value, the surface of the absorbent became positively charged owing to the protonation. While the pH value was higher than 7.4, the grafted amine ligand was deprotonated and gained a negatively charge.

Batch adsorption experiments were performed and the adsorption performance of SBA-15-DETA at different pH values was studied. As exhibited in Fig. 7b, the adsorbed amount of Cu(II) increased gradually as the pH of the suspension increased from 2.0 to 7.0. Besides, when the pH increased, the adsorption of Cr(III) increased slowly at pH < 6.0, followed by an abrupt increase at pH 6.0–7.0, and then reached a plateau at pH 7.0–8.0. Thus, the change

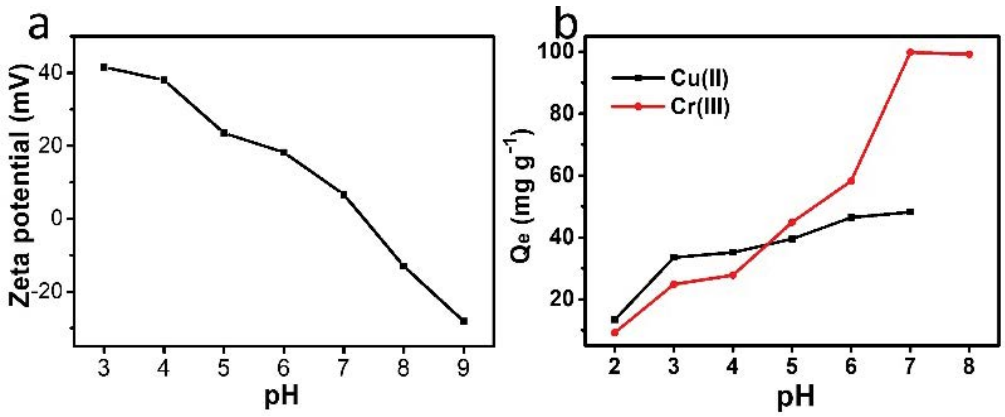

Fig. 7. (a) Apparent zeta-potential values of the SBA-15-DETA as a function of solution pH values (0.01 g SBA-15-DETA, 100 mL of 0.1 mmol/L NaCl solution, and the pH values were adjusted by NaOH and HCl) and (b) effect of pH on the adsorption capacity of SBA-15-DETA toward Cu(II) and Cr(III) (40 mg of SBA-15-DETA, 40.0 mL of 100 mg/L initial ions solution, temperature 25°C, and contact time 5 h).

of adsorption capacity for Cr(III) was much greater than that for Cu(II) with the increasing pH values. The difference between the adsorption capacity for Cu(II) and Cr(III) ions was dependent on the pH values of experimental conditions. The pH-dependent ions removal was not only influenced by the effect of protonation, but also by the effect of hydrolysis of ions. At a low pH value, protons in an acidic solution could protonate the binding sites of the grafted amine ligands, resulting in the decrease of metal ions binding. When the pH value was high, the hydroxide in a basic solution may complex and precipitate metal ions. At pH 2.0–3.0, $[Cr(H_2O)_6]^{3+}$ was the major species [36]. When the pH increased in the pH range of 3.0–6.0, more reactive OH^- displaced the water molecules to form other species including $Cr(H_2O)_2OH^{2+}$ and $Cr(H_2O)(OH)^{2+}$. Besides, for the adsorption of Cu(II), it was reported that the precipitation of Cu(II) as hydroxide may occur at pH 6.0 [37]. Thus, to avoid hydrolyzing of Cu(II) and Cr(III), the pH values of two suspensions were selected at 5.0 and 3.0 as the optimum adsorption condition, respectively.

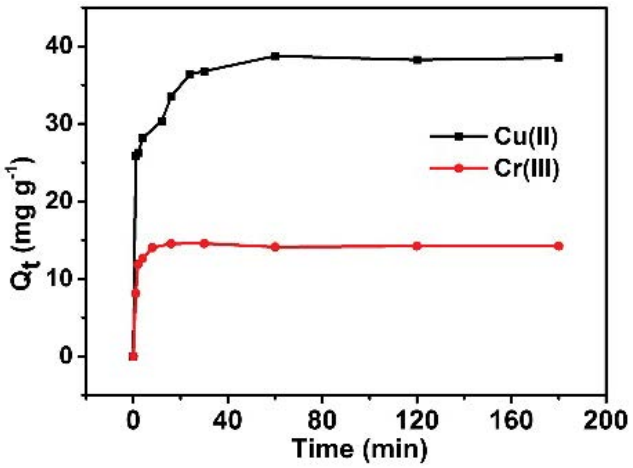

Fig. 8. Adsorption rates of SBA-15-DETA for Cu(II) and Cr(III) (40 mg of SBA-15-DETA, 40.0 mL of 100 mg/L initial ions solution, pH 5.0 for Cu(II)/pH 3.0 for Cr(III), and temperature 25°C).

3.3. Effect of contact time

The adsorption trend of SBA-15-DETA for Cu(II) and Cr(III) at different contact time was studied. As shown in Fig. 8, sorption of Cu(II) on SBA-15-DETA was faster than that of Cr(III) at the fixed time. The result also showed adsorption rates of Cu(II) and Cr(III) were very fast at the initial adsorption period, then increased gradually and finally leveled off to reach adsorption equilibrium. It could be explained that with the adsorption process going on, both ion concentrations in the aqueous solution and the amount of available functional groups on the absorbents decreased over time, leading to the slowdown of adsorption rate and final state of adsorption equilibrium.

According to the adsorption trend, the time for achieving optimum was 60 min for Cu(II), and 20 min for Cr(III). In addition, it was evident that ion removal efficiency of Cr(III) on SBA-15-DETA was much lower than that of Cu(II) at optimum adsorption, when 100 mg L^{-1} of ions solutions were used for adsorption. The fast adsorption equilibrium is beneficial for effective application of the material. The rapid uptake indicated a high affinity between the chelating ligand and heavy metal ions. It can be explained that the surface of SBA-15-DETA became hydrophilic after modification with the branched amine. In addition, the large BET surface area and high pore volume of the absorbent were also favorable for the rapid diffusion of adsorbates inside. In order to ensure the attainment of adsorption equilibrium, 180 min of the shaking time was chosen in the following experiments.

Kinetics analysis for metal ions uptake is able to provide essential information on adsorption mechanism [32]. The commonly used pseudo-first-order and pseudo-second-order kinetic equations were used here to interpret the kinetic characteristics of the metal adsorption of SBA-15-DETA. Pseudo-first-order [38] and pseudo-second-order [39] kinetic models are generally described as the following equations:

$$\log\left(Q_e - Q_t\right) = -\frac{k_1}{2.303}t + \log Q_e \quad (1)$$

$$\frac{t}{Q_t} = \frac{1}{k_2 Q_e^2} + \frac{t}{Q_e} \quad (2)$$

where Q_e (mg g^{-1}) and Q_t (mg g^{-1}) are the amount of metal ions adsorbed at the equilibrium state and at the predetermined contact time t (min), respectively, while k_1 (min^{-1}) and k_2 (g mg^{-1} min^{-1}) refer to the rate constants of the pseudo-first-order and pseudo-second-order kinetic model, respectively. By plotting $\log(Q_e - Q_t)$ vs. t (pseudo-first-order) and t/Q_t vs. t (pseudo-second-order), the fitting curves and their estimated parameter values were obtained and presented in Fig. 9 and Table 2, respectively. The experimental data for Cu(II) and Cr(III) fitted the pseudo-second-order model better than the pseudo-first-order model since the value of correlation coefficients (R^2) of pseudo-second-order model was much higher and close to 1. Besides, as compared with the values obtained from the pseudo-first-order model, calculated equilibrium adsorption capacity from pseudo-second-order model were more consistent with the final adsorption results According to the hypothesis of pseudo-second-order model [25], it is possible that ion uptake was a chemical adsorption process between metal ions and the adsorbents due to valence forces via exchange or sharing of electrons.

3.4. Effect of initial concentration

Equilibrium studies on both SBA-15-DETA and SBA-15-NH_2 using varying concentrations of two ions were performed and adsorption trends are shown in Fig. 10. It shows the adsorption capacities of both SBA-15-NH_2 and SBA-15-DETA for Cu(II) and Cr(III) ions increased gradually upon the increasing initial metal ions concentration. When the initial Cu(II) and Cr(III) ions concentration was 400 mg L^{-1}, the maximum adsorption capacity of SBA-15-DETA reached 54.2 mg g^{-1} for Cu(II) and 36.5 mg g^{-1} for Cr(III), respectively. Thus, it can be concluded that the SBA-15-DETA had better adsorption efficiency than that of the silica precursor SBA-15-NH_2 toward the two ions. Given the branched amine have been introduced to the adsorbent after amidation, the improved adsorption performance could mean that SBA-15-DETA featured more available binding sites than that of SBA-15-NH_2.

In order to elucidate the mechanism that adsorption occurred, the commonly used Langmuir and Freundlich isotherm models [40] were used and described as the following equations:

$$\frac{C_e}{Q_e} = \frac{C_e}{Q_m} + \frac{1}{Q_m \times K_L} \quad (3)$$

$$\log Q_e = \log K_F + \frac{1}{n}\log C_e \quad (4)$$

where Q_e (mg g^{-1}) and Q_m (mg g^{-1}) are equilibrium adsorption capacity and theoretical maximum adsorption capacity of the adsorbent, respectively, C_e (mg L^{-1}) represents the equilibrium metal ion concentration after adsorption (mg L^{-1}), K_L (L mg^{-1}) is the Langmuir affinity constant, K_F (mg g^{-1}) refers to the Freundlich constant associated with the

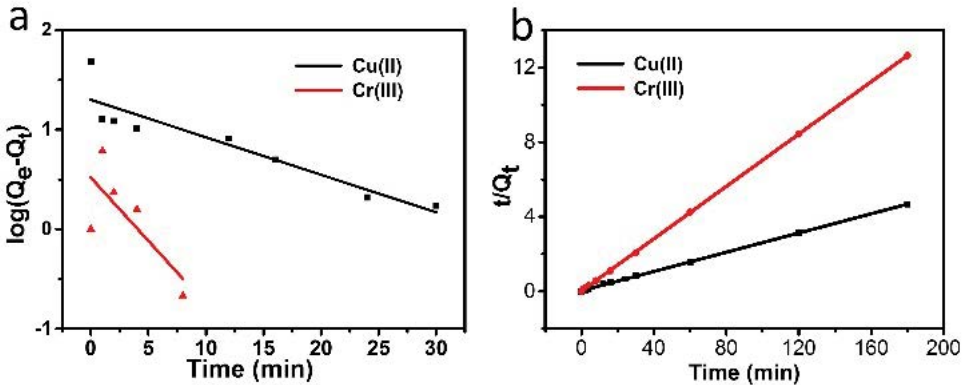

Fig. 9. Kinetic linear fitting plots of (a) pseudo-first-order and (b) pseudo-second-order kinetic model for Cu(II) and Cr(III) adsorption on SBA-15-DETA.

Table 2
Kinetic parameters of pseudo-first-order and pseudo-second-order models for adsorption

Metal ions	Pseudo-first-order			Pseudo-second-order		
	k_1 (min^{-1})	Q_e (mg g^{-1})	R^2	k_2 (g mg^{-1} min^{-1})	Q_e (mg g^{-1})	R^2
Cu(II)	0.09	20.0	0.829	0.02	38.8	0.999
Cr(III)	0.29	3.3	0.418	0.39	14.2	0.999

adsorption capacity, and n is the heterogeneity factor related to sorption intensity.

By plotting C_e/Q_e against C_e (Langmuir model) and $\log Q_e$ against $\log C_e$ (Freundlich model), their fitting curves are shown in Figs. 11 and 12. Besides, the corresponding Langmuir and Freundlich isotherm parameters are obtained and shown in Table 3. The results reveal that the metal ions adsorption isotherms can be better described by the Langmuir isotherm model than the Freundlich model, based on the comparatively higher value of its correlation

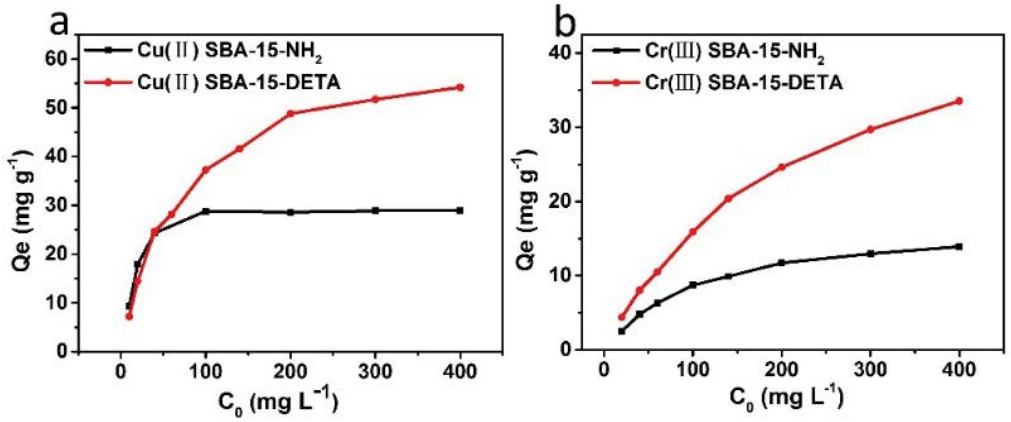

Fig. 10. Effect of initial (a) Cu(II) and (b) Cr(III) concentration on adsorption capacity of SBA-15-NH_2 and SBA-15-DETA (40 mg of adsorbent, 40.0 mL of 100 mg/L initial ions solution, pH 5.0 for Cu(II)/pH 3.0 for Cr(III), and temperature 25°C).

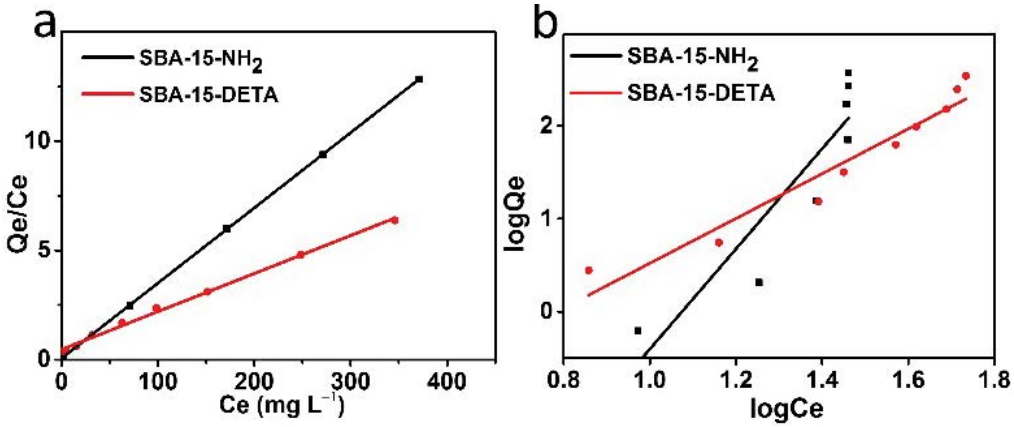

Fig. 11. Linear isotherms fitting plots of (a) Langmuir model and (b) Freundlich model for the adsorption of Cu(II).

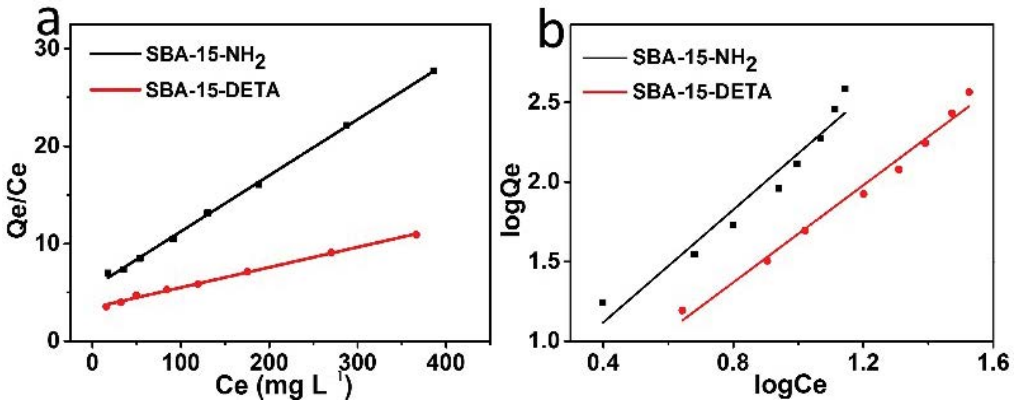

Fig. 12. Linear isotherms fitting plots of (a) Langmuir model and (b) Freundlich model for the adsorption of Cr(III).

Table 3
Langmuir and Freundlich isotherm parameters

Adsorbent	Metal ions	Langmuir model			Freundlich model		
		K_L (L mg^{-1})	Q_m (mg g^{-1})	R^2	n	K_F (mg g^{-1})	R^2
SBA-15-NH_2	Cu(II)	5.92×10^{-1}	29.1	0.998	2.01	3.35	0.686
	Cr(III)	1.04×10^{-2}	17.4	0.999	1.79	0.58	0.942
SBA-15-DETA	Cu(II)	3.77×10^{-2}	57.5	0.998	3.92	7.31	0.941
	Cr(III)	6.01×10^{-3}	48.3	0.999	1.48	0.63	0.971

coefficients. According to the theory of the Langmuir model [41], it is likely that all the active sites of SBA-15-DETA were homogenously distributed and monolayer sorption occurred on the surface of the material. Meanwhile, the branched amine ligand grafted on SBA-15 reacted with metal ions through a complexation mechanism. According to Langmuir fitting curves, the maximum adsorption capacities of SBA-15-NH_2 and SBA-15-DETA toward Cu(II)/Cr(III) were 29.1/17.4 and 57.5/48.3 mg g^{-1}, respectively. Considering the adsorption capacity of SBA-15-DETA toward the two ions was much higher than that of SBA-15-NH_2, it is believed that the increasing density of branched chelating groups is beneficial for improving adsorption performance toward heavy metals in this study.

Elemental analysis was used to directly evaluate the nitrogen content of samples. The nitrogen contents of pristine SBA-NH_2 and SBA-15-DETA were determined to be 1.1 and 3.6 mmol/g, respectively. It can be concluded that the adsorption performance of SBA-NH_2 and SBA-15-DETA increased with the increasing nitrogen contents. Moreover, the maximum adsorption capacity of SBA-15-NH_2 could be converted to 0.45 mmol/g for Cu(II) and 0.33 mmol/g for Cr(III). Thus, most of the functional nitrogen atoms on SBA-NH_2 seemed to form 2.4:1 complex with Cu(II) and 3.3:1 complex with Cr(III). On the other hand, the maximum adsorption capacity of SBA-15-DETA were 0.90 mmol/g for Cu(II) and 0.93 mmol/g for Cr(III). The molar ratio of nitrogen atoms with respect to Cu(II) and Cr(III) was calculated to be 4.0:1 and 3.8:1, respectively. According to the above fact, the adsorbents with a high content of nitrogen element led to the increase of N to adsorbed ions ratios, which may be attributed to the higher steric hindrance effect of the grafted ligands.

3.5. X-ray diffraction analyses

To investigate the interactions between SBA-15-DETA and heavy metal ions, XPS analysis of the surface of adsorbents before and after ions adsorption was conducted. Wide scan XPS spectra of SBA-15-DETA before and after Cu(II) and Cr(III) adsorption are displayed in Fig. 13a. The appearance of the Cu(II) and Cr(III) binding energy peaks at 935 and 577/586 nm after adsorption were observed and these results confirmed the successful uptake of ions by SBA-15-DETA. The narrow N 1s spectrum of SBA-15-DETA comprised two peaks (Fig. 13b). The peak at 398.8 eV was attributed to the nitrogen in primary/secondary/tertiary amine and amide groups, while the second weak peak at 400.6 eV mainly originated from protonated amine. As shown in Fig. 13c, a new peak appeared at 401.6 eV, and the peak at 398.8 eV of SBA-15-DETA shifted slightly to 399.7 eV after Cu(II) adsorption. Besides, after Cr(III) adsorption, the peak at 398.8 eV of SBA-15-DETA shifted slightly to 401.5 eV, and two new peaks appeared at 401.5 and 406.5 eV (Fig. 13d). The peak at 406.5 eV might correspond to the NO_3^- anion attracted by the protonated amine on SBA-15-DETA, when the adsorbents were incubated with $Cr(NO_3)_3$ for adsorption. These results demonstrate that adsorption was probably caused by the coordination interaction between the amine ligand and Cu(II)/Cr(III) metal ions. Therefore, a possible binding mechanism of SBA-15-DETA with Cu(II)/Cr(III) ions is proposed and exhibited in Fig. 14.

3.6. Effect of ionic strength

The influence of ionic strength was also examined and $NaNO_3$ was select as the representative salt. As shown in Fig. 15, with the increasing ionic strength from 0 to 1.0 mol/L of $NaNO_3$, only a slight decrease of Cu(II) adsorption amount from 39.6 to 36.5 mg g^{-1} and Cr(III) adsorption amount from 21.5 to 19.6 mg g^{-1} was observed. On the whole, ion strength increase did not inhibit the Cu(II) and Cr(III) adsorption at the described concentration range. Thus, the added Na(I) did not interact with amine groups to interfere adsorption process and the complexation may be the main factor responsible for ions adsorption.

3.7. Adsorption selectivity

Since a broad range of cations may coexisted in real water samples, it is very important to study the influence of various ions for the adsorption property of SBA-15-DETA. The selective adsorption of Cu(II) and Cr(III) ions was studied using a medium that contained metal ions including Cu(II), Cr(III), Co(II), Ni(II), Cd(II), Mn(II), and Na(I). In order to be consistent with previous experimental conditions, the completive study was performed at pH 3.0 and 5.0, respectively, and the results are shown in Fig. 16. When the suspension pH was 3.0, adsorbed amount of Cu(II) and Cr(III) were much higher than that of other coexisted metal ions, and the adsorption was selective toward Cu(II) and Cr(III) ions. The adsorption performance of SBA-15-DETA for all the studied ions other than Na(I) increased significantly when the pH value increased to 5.0. At this time, the selectivity towards Cu(II) and Cr(III) ions with respect to Co(II), Ni(II), Cd(II), and Mn(II) decreased. Therefore, the adsorption method is selective for Cu(II) and Cr(III) ions

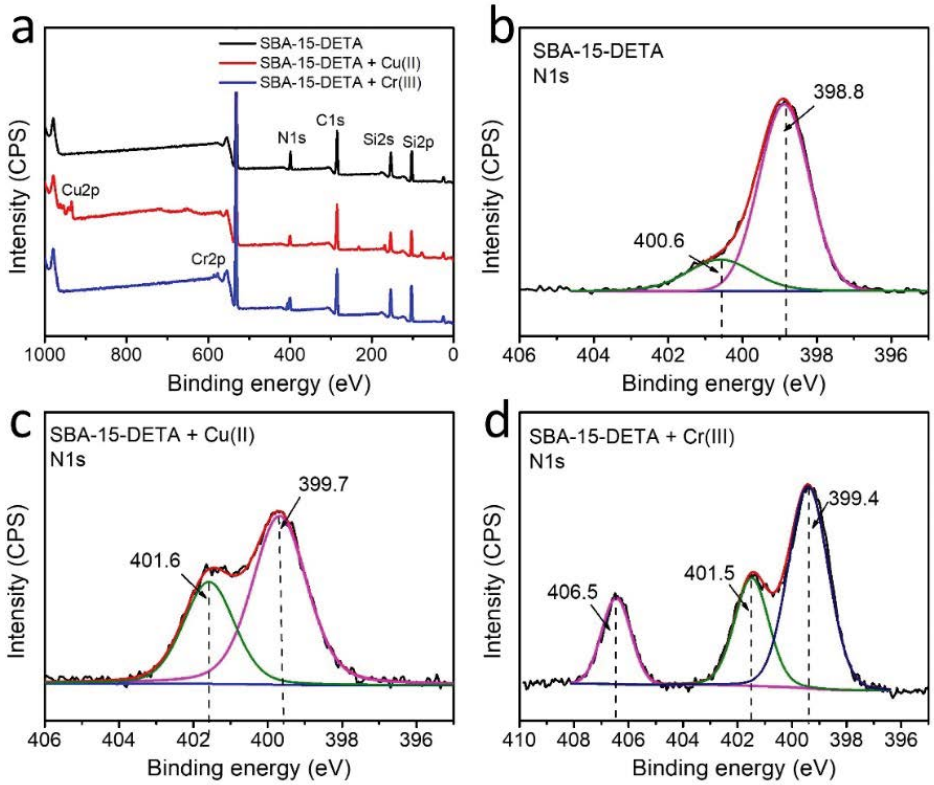

Fig. 13. (a) XPS spectra of SBA-15-DETA before and after adsorption of metal ions, (b) N 1s spectrum of SBA-15-DETA before adsorption, N 1s spectra of SBA-15-DETA after adsorption of (c) Cu(II), and (d) Cr(III) ions.

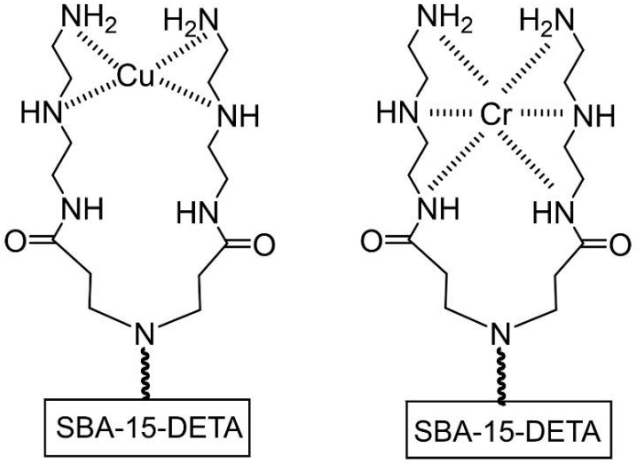

Fig. 14. Possible mechanism of Cu(II) and Cr(III) coordination by branched amine on SBA-15-DETA.

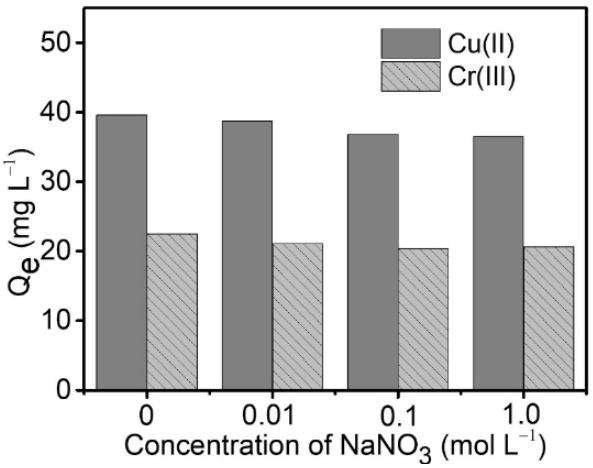

Fig. 15. Effects of ionic strength ($NaNO_3$) on Cu(II) and Cr(III) adsorption (40 mg of adsorbent, 40.0 mL of 100 mg/L initial ions solution, pH 5.0 for Cu(II)/pH 3.0 for Cr(III), and temperature 25°C).

at pH 3.0, although the adsorption performance of SBA-15-DETA toward the two ions is lower than that at pH 5.0.

3.8. Reusability study

The reusability of the adsorbent is a key feature for practical application. Initially, the metal ions adsorbed SBA-15-DETA was collected by centrifugation. The previous pH study revealed that the amount of adsorbed ions was very low under strong acidic conditions. Thus, 0.1 mol L^{-1} HCl was selected as the desorption reagent. As exhibited in Fig. 17, the adsorption capacity was still above 90% of the original value after four adsorption–desorption cycles, indicating that branched amine functionality firmly immobilized on the silica and the adsorption performance could be well-maintained during the regeneration process.

Table 4
Comparison of adsorption capacity with other SBA-15 adsorbents

Adsorbent	Ions	pH	Q_e (mg g^{-1})	Reference
NH_2-SBA-15-f	Cu(II)	6.0	19.8	[20]
G-SBA-15-NN-E	Cu(II)	Unmentioned	53.1	[17]
MDA–SBA-15	Cu(II)	4.0	90.3	[30]
SA-SBA-15	Cu(II)	4.8	57.2	[42]
TS-SBA-15	Cr(III)	6.0	31.0	[43]
SBA-15-Cr(III)-IIP	Cr(III)	6.0	38.5	[44]
G3-PAMAM-SBA-15	Cr(III)	4.0	23.0	[45]
DPP@SBA-15	Cr(III)	6.0	72.5	[19]
SBA-15-DETA	Cu(II)	5.0	57.5	This study
SBA-15-DETA	Cr(III)	3.0	48.3	This study

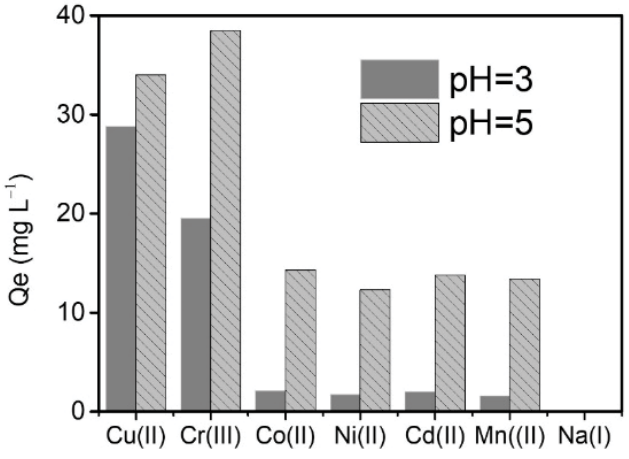

Fig. 16. Competitive adsorption of coexistent ions on SBA-15-DETA in mixed metal ion solutions (80 mg of adsorbent, 80.0 mL of 100 mg/L each initial ion solution, and temperature 25°C).

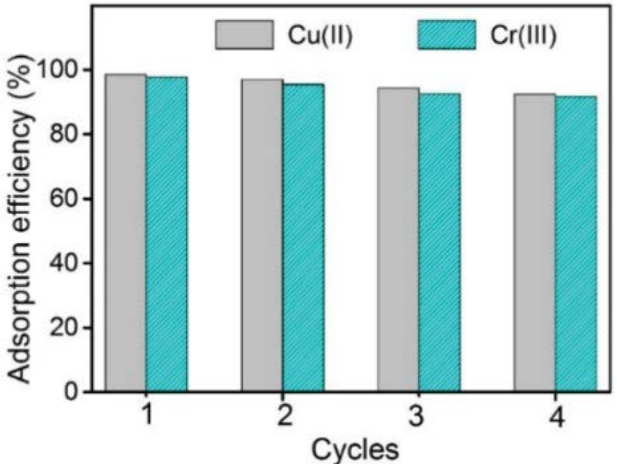

Fig. 17. Reusability of SBA-15-DETA toward the adsorption of Cu(II) or Cr(III) with four adsorption–desorption cycles (40 mg of SBA-15-DETA, 40.0 mL of 100 mg/L initial ions solution, pH 5.0 for Cu(II)/pH 3.0 for Cr(III), and temperature 25°C).

3.9. Comparison with some other adsorbents

Adsorption capacity of the SBA-15-DETA toward both cations were compared with other mesoporous silica adsorbents. The adsorption performances of various adsorbents are summarized in Table 4. It can be observed the adsorption capacity value of SBA-15-DETA for Cu(II) and Cr(III) was relatively higher than or similar to those of other adsorbents [17,20,43–45], but lower than some adsorbents bearing branched chelating ligands [19,30].

4. Conclusion

In this study, the branched amine moiety was successfully immobilized onto the surfaces of SBA-15 mesoporous silica. Adsorption behavior of SBA-15-DETA for the removal of Cu(II) and Cr(III) ions from water was investigated via batch adsorption tests. The effects of the solution pH, contact time, and initial metal ion concentration were investigated. According to the results, the introduction of branched amine to the SBA-15-NH_2 precursor could increase the adsorption performance of the adsorbent. The adsorption kinetic was better represented by the pseudo-second-order kinetic model. Besides, Langmuir isotherm model fitted experimental data adsorption isotherm, indicating adsorption sites on the adsorbent were homogeneous and adsorption occurred on monolayer. SBA-15-DETA also exhibited a measure of selective adsorption performance toward Cu(II) and Cr(III) ions in the mixed metal ions solution. In addition, with excellent regeneration and reuse performance, this absorbent presents a great potential for removing toxic metal ions from wastewater.

Acknowledgments

This work was financially supported by the Natural Science Foundation of Jiangsu Province (No. BK20171263), the Priority Academic Program Development of Jiangsu Higher Education Institutions (PAPD), Postgraduate Research and Practice Innovation Program of Jiangsu Province (KYCX18-2603), and Innovation and Entrepreneurship Training Program for College Students of Jiangsu Province (201811641023Z).

References

[1] D.W. O'Connell, C. Birkinshaw, T.F. O'Dwyer, Heavy metal adsorbents prepared from the modification of cellulose: a review, Bioresour. Technol., 99 (2008) 6709–6724.

[2] G. Zhao, X. Huang, Z. Tang, Q. Huang, F. Niu, X. Wang, Polymer-based nanocomposites for heavy metal ions removal from aqueous solution: a review, Polym. Chem., 9 (2018) 3562–3582.

[3] C.F. Carolin, P.S. Kumar, A. Saravanan, G.J. Joshiba, M. Naushad, Efficient techniques for the removal of toxic heavy metals from aquatic environment: a review, J. Environ. Chem. Eng., 5 (2017) 2782–2799.

[4] F. Fu, Q. Wang, Removal of heavy metal ions from wastewaters: a review, J. Environ. Manage., 92 (2011) 407–418.

[5] S. Sen Gupta, K.G. Bhattacharyya, Kinetics of adsorption of metal ions on inorganic materials: a review, Adv. Colloid Interface Sci., 162 (2011) 39–58.

[6] E. Da'na, Adsorption of heavy metals on functionalized-mesoporous silica: a review, Microporous Mesoporous Mater., 247 (2017) 145–157.

[7] V.B. Cashin, D.S. Eldridge, A. Yu, D. Zhao, Surface functionalization and manipulation of mesoporous silica adsorbents for improved removal of pollutants: a review, Environ. Sci. Water Res. Technol., 4 (2018) 110–128.

[8] M.H. Dindar, M.R. Yaftian, S. Rostamnia, Potential of functionalized SBA-15 mesoporous materials for decontamination of water solutions from Cr(VI), As(V) and Hg(II) ions, J. Environ. Chem. Eng., 3 (2015) 986–995.

[9] L. Dolatyari, M.R. Yaftian, S. Rostamnia, Removal of Uranium(VI) ions from aqueous solutions using Schiff base functionalized SBA-15 mesoporous silica materials, J. Environ. Manage., 169 (2016) 8–17.

[10] Z. Dousti, L. Dolatyari, M.R. Yaftian, S. Rostamnia, Adsorption of Eu(III), Th(IV), and U(VI) by mesoporous solid materials bearing sulfonic acid and sulfamic acid functionalities, Sep. Sci. Technol., 54 (2019) 2609–2624.

[11] J.-K. Kang, J.-H. Kim, S.-B. Kim, S.-H. Lee, J.-W. Choi, C.-G. Lee, Ammonium-functionalized mesoporous silica MCM-41 for phosphate removal from aqueous solutions, Desal. Water Treat., 57 (2016) 10839–10849.

[12] J.-K. Kang, J.-A. Park, J.-H. Kim, C.-G. Lee, S.-B. Kim, Surface functionalization of mesoporous silica MCM-41 with 3-aminopropyltrimethoxysilane for dye removal: kinetic, equilibrium, and thermodynamic studies, Desal. Water Treat., 57 (2016) 7066–7078.

[13] P.N.E. Diagboya, E.D. Dikio, Silica-based mesoporous materials; emerging designer adsorbents for aqueous pollutants removal and water treatment, Microporous Mesoporous Mater., 266 (2018) 252–267.

[14] D.H. Shin, Y.G. Ko, U.S. Choi, W.N. Kim, Design of high efficiency chelate fibers with an amine group to remove heavy metal ions and pH-related FT-IR analysis, Ind. Eng. Chem. Res., 43 (2004) 2060–2066.

[15] E. Da'na, A. Sayari, Adsorption of copper on amine-functionalized SBA-15 prepared by co-condensation: equilibrium properties, Chem. Eng. J., 166 (2011) 445–453.

[16] L. Zhang, C. Yu, W. Zhao, Z. Hua, H. Chen, L. Li, J. Shi, Preparation of multi-amine-grafted mesoporous silicas and their application to heavy metal ions adsorption, J. Non-Cryst. Solids, 353 (2007) 4055–4061.

[17] J. Aguado, J.M. Arsuaga, A. Arencibia, M. Lindo, V. Gascón, Aqueous heavy metals removal by adsorption on amine-functionalized mesoporous silica, J. Hazard. Mater., 163 (2009) 213–221.

[18] T. Kang, Y. Park, K. Choi, J.S. Lee, J. Yi, Ordered mesoporous silica (SBA-15) derivatized with imidazole-containing functionalities as a selective adsorbent of precious metal ions, J. Mater. Chem., 14 (2004) 1043–1049.

[19] S. Liu, H.-Z. Cui, Y.-L. Li, A.-L. Yang, J.-F. Zhang, R. Zhong, Q. Zhou, M. Lin, X.-F. Hou, Bis-pyrazolyl functionalized mesoporous SBA-15 for the extraction of Cr(III) and detection of Cr(VI) in artificial jewelry samples, Microchem. J., 131 (2017) 130–136.

[20] J.-Y. Lee, C.-H. Chen, S. Cheng, H.-Y. Li, Adsorption of Pb(II) and Cu(II) metal ions on functionalized large-pore mesoporous silica, Int. J. Environ. Sci. Technol., 13 (2016) 65–76.

[21] Z.A. Alothman, A.W. Apblett, Preparation of mesoporous silica with grafted chelating agents for uptake of metal ions, Chem. Eng. J., 155 (2009) 916–924.

[22] S. Wang, K. Wang, C. Dai, H. Shi, J. Li, Adsorption of Pb^{2+} on amino-functionalized core–shell magnetic mesoporous SBA-15 silica composite, Chem. Eng. J., 262 (2015) 897–903.

[23] P.N. Diagboya, B.I. Olu-Owolabi, K.O. Adebowale, Microscale scavenging of pentachlorophenol in water using amine and tripolyphosphate-grafted SBA-15 silica: batch and modeling studies, J. Environ. Manage., 146 (2014) 42–49.

[24] C.-H. Yen, H.-L. Lien, J.-S. Chung, H.-D. Yeh, Adsorption of precious metals in water by dendrimer modified magnetic nanoparticles, J. Hazard. Mater., 322 (2017) 215–222.

[25] B. Hayati, A. Maleki, F. Najafi, F. Gharibi, G. McKay, V.K. Gupta, S. Harikaranahalli Puttaiah, N. Marzban, Heavy metal adsorption using PAMAM/CNT nanocomposite from aqueous solution in batch and continuous fixed bed systems, Chem. Eng. J., 346 (2018) 258–270.

[26] E.-Y. Jeong, M.B. Ansari, Y.-H. Mo, S.-E. Park, Removal of Cu(II) from water by tetrakis(4-carboxyphenyl) porphyrin-functionalized mesoporous silica, J. Hazard. Mater., 185 (2011) 1311–1317.

[27] Z. Ezzeddine, I. Batonneau-Gener, Y. Pouilloux, H. Hamad, Z. Saad, V. Kazpard, Divalent heavy metals adsorption onto different types of EDTA-modified mesoporous materials: effectiveness and complexation rate, Microporous Mesoporous Mater., 212 (2015) 125–136.

[28] S. Nayab, A. Farrukh, Z. Oluz, E. Tuncel, S.R. Tariq, H.U. Rahman, K. Kirchhoff, H. Duran, B. Yameen, Design and fabrication of branched polyamine functionalized mesoporous silica: an efficient absorbent for water remediation, ACS Appl. Mater. Interfaces, 6 (2014) 4408–4417.

[29] Y. Pang, G. Zeng, L. Tang, Y. Zhang, Y. Liu, X. Lei, Z. Li, J. Zhang, G. Xie, PEI-grafted magnetic porous powder for highly effective adsorption of heavy metal ions, Desalination, 281 (2011) 278–284.

[30] A. Shahbazi, H. Younesi, A. Badiei, Functionalized SBA-15 mesoporous silica by melamine-based dendrimer amines for adsorptive characteristics of Pb(II), Cu(II) and Cd(II) heavy metal ions in batch and fixed bed column, Chem. Eng. J., 168 (2011) 505–518.

[31] M. Anbia, K. Kargosha, S. Khoshbooei, Heavy metal ions removal from aqueous media by modified magnetic mesoporous silica MCM-48, Chem. Eng. Res. Des., 93 (2015) 779–788.

[32] S. Ravi, Y.-R. Lee, K. Yu, J.-W. Ahn, W.-S. Ahn, Benzene triamido-tetraphosphonic acid immobilized on mesoporous silica for adsorption of Nd^{3+} ions in aqueous solution, Microporous Mesoporous Mater., 258 (2018) 62–71.

[33] J. Villarroel Rocha, D. Barrera, K. Sapag, Improvement in the pore size distribution for ordered mesoporous materials with cylindrical and spherical pores using the Kelvin equation, Top. Catal., 54 (2011) 121–134.

[34] A. Sayari, B.-H. Han, Y. Yang, Simple synthesis route to monodispersed SBA-15 silica rods, J. Am. Chem. Soc., 126 (2004) 14348–14349.

[35] R.P. Mohubedu, P.N.E. Diagboya, C.Y. Abasi, E.D. Dikio, F. Mtunzi, Magnetic valorization of biomass and biochar of a typical plant nuisance for toxic metals contaminated water treatment, J. Cleaner Prod., 209 (2019) 1016–1024.

[36] J. Pan, J. Jiang, R. Xu, Adsorption of Cr(III) from acidic solutions by crop straw derived biochars, J. Environ. Sci., 25 (2013) 1957–1965.

[37] X.-j. Tong, J.-y. Li, J.-h. Yuan, R.-k. Xu, Adsorption of Cu(II) by biochars generated from three crop straws, Chem. Eng. J., 172 (2011) 828–834.

[38] H. Yuh-Shan, Citation review of Lagergren kinetic rate equation on adsorption reactions, Scientometrics, 59 (2004) 171–177.

[39] Y.S. Ho, G. McKay, Pseudo-second order model for sorption processes, Process Biochem., 34 (1999) 451–465.
[40] Y.S. Ho, C.C. Chiang, Sorption studies of acid dye by mixed sorbents, Adsorption, 7 (2001) 139–147.
[41] P.K. Tapaswi, M.S. Moorthy, S.S. Park, C.-S. Ha, Fast, selective adsorption of Cu^{2+} from aqueous mixed metal ions solution using 1,4,7-triazacyclononane modified SBA-15 silica adsorbent (SBA-TACN), J. Solid State Chem., 211 (2014) 191–199.
[42] M. Mureseanu, A. Reiss, I. Stefanescu, E. David, V. Parvulescu, G. Renard, V. Hulea, Modified SBA-15 mesoporous silica for heavy metal ions remediation, Chemosphere, 73 (2008) 1499–1504.
[43] S. Parambadath, A. Mathew, M.J. Barnabas, S.Y. Kim, C.-S. Ha, Concentration-dependant selective removal of Cr(III), Pb(II) and Zn(II) from aqueous mixtures using 5-methyl-2-thiophenecarboxaldehyde Schiff base-immobilised SBA-15, J. Sol-Gel Sci. Technol., 79 (2016) 426–439.
[44] Y. Liu, X. Meng, J. Han, Z. Liu, M. Meng, Y. Wang, R. Chen, S. Tian, Speciation, adsorption and determination of chromium(III) and chromium(VI) on a mesoporous surface imprinted polymer adsorbent by combining inductively coupled plasma atomic emission spectrometry and UV spectrophotometry, J. Sep. Sci., 36 (2013) 3949–3957.
[45] Y. Jiang, Q. Gao, H. Yu, Y. Chen, F. Deng, Intensively competitive adsorption for heavy metal ions by PAMAM-SBA-15 and EDTA-PAMAM-SBA-15 inorganic–organic hybrid materials, Microporous Mesoporous Mater., 103 (2007) 316–324.